



Contents lists available at ScienceDirect

International Journal of Applied Earth Observations and Geoinformation

journal homepage: www.elsevier.com/locate/jag

Evaluation and comparison of light use efficiency models for their sensitivity to the diffuse PAR fraction and aerosol loading in China

Xin Li^{a,b}, Hongyu Liang^{c,*}, Weiming Cheng^a^a State Key Laboratory of Resources and Environmental Information System, Institute of Geographic Sciences and Natural Resources Research, Chinese Academy of Sciences, Beijing 100049, China^b The Image Sky International Co., Ltd, China^c The Department of Land Surveying and Geo-Informatics, The Hong Kong Polytechnic University, 999077, Hong Kong, China

ARTICLE INFO

Keywords:

PAR_{diff} fraction
 Aerosol optical depth (AOD)
 Gross primary productivity (GPP)
 Sensitivity

ABSTRACT

The diffuse photosynthetically active radiation (PAR_{diff}) is highly related to the gross primary productivity (GPP) of vegetation and can enhance the photosynthetic rate of shaded leaves. The PAR_{diff} is mainly influenced by aerosols on clear sky days. To explore the impacts of the PAR_{diff} fraction and aerosol loading on the accuracy of GPP estimations, we evaluated and compared the sensitivity of one-leaf and two-leaf light use efficiency (LUE) models (MOD17 and TL-LUE models) to the PAR_{diff} fraction and aerosol optical depth (AOD) using satellite data and measurements at ChinaFLUX sites in China from 2003 to 2010. The estimated GPP from two models (GPP_{MOD} and GPP_{TL}) showed systematic underestimations when compared with the measured GPP at ChinaFLUX sites (GPP_{FLUX}). In addition, the underestimation of the GPP estimated by the two models was larger in months with high PAR_{diff} fractions than in months with low PAR_{diff} fractions at most sites. The TL-LUE model exhibited better performance than the MOD17 model with reduced underestimation and root-mean-square error (RMSE) values when the PAR_{diff} fraction was greater than 0.7 or 0.8. When the PAR_{diff} fraction was low, the TL-LUE model reduced the overestimation or increased the underestimations of GPP compared with the MOD17 model depending on the site. Both MOD17 and TL-LUE exhibited higher underestimations of GPP at high AOD values than at low AOD values at most sites. The TL-LUE model exhibited an overall better performance than MOD17 under high AOD. The overestimation also occurred for low AOD, which was consistent with that for low PAR_{diff} fractions. Therefore, the two LUE models showed dynamic performance with variations in the PAR_{diff} fraction and AOD, which should be considered in the application and further improvement of GPP models.

1. Introduction

Terrestrial gross primary production (GPP), which represents the amount of carbon absorbed from the atmosphere and fixed by land vegetation, plays a vital role in the terrestrial carbon cycle (He et al. 2013; Sun et al. 2019; Yan et al. 2017). The GPP is also important for the water cycles and energy balance throughout almost all ecosystem processes (Sun et al. 2019; Tramontana et al. 2015; Yan et al. 2017). Therefore, accurate and reliable GPP estimations are necessary for understanding the carbon cycle and predicting plant production (Cheng et al. 2014; Yuan et al. 2014).

The GPP estimation models can be generally categorized as process-based ecological models and remote sensing (RS)-based light use efficiency (LUE) models (He et al. 2013). The LUE models driven by remote

sensing data are more widely used for GPP retrievals on a large scale than ecological models because of the vast coverage and few required inputs (Zan et al. 2018). As a popular LUE model, the MOD17 model produces global GPP in near real time based on absorbed photosynthetically active radiation (APAR) and LUE by incorporating environmental stress factors, such as temperature and water vapor pressure deficit (Yuan et al. 2014). However, the MOD17 model is a one-leaf model, which assumes that the canopy acts as a large leaf and GPP has a linear relationship with incident photosynthetically active radiation (PAR, 400–700 nm) (Zan et al. 2018). However, the exposure to PAR and LUE is different for sunlit and shaded leaves. Specifically, sunlit leaves can absorb both direct and diffuse PAR (PAR_{dir} and PAR_{diff}) and are easily saturated by light, which results in a low LUE under clear sky conditions, whereas shaded leaves absorb only diffuse PAR, which leads

* Corresponding author at: The Department of Land Surveying and Geo-Informatics, The Hong Kong Polytechnic University, Hong Kong, China.
 E-mail address: allenhongyu.liang@connect.polyu.hk (H. Liang).

<https://doi.org/10.1016/j.jag.2020.102269>

Received 25 May 2020; Received in revised form 15 August 2020; Accepted 30 October 2020

Available online 2 December 2020

0303-2434/© 2020 The Author(s).

Published by Elsevier B.V. This is an open access article under the CC BY-NC-ND license

(<http://creativecommons.org/licenses/by-nc-nd/4.0/>).

Table 1
Location and vegetation cover of the eight ChinaFLUX sites.

Sites	YC	CBS	QYZ	DHS	XSBN	HB	NMG	DX
Lat (°)	36.83	42.40	26.741	23.173	21.928	37.610	43.326	30.469
Lon (°)	116.57	128.10	115.058	112.536	101.265	101.322	116.404	91.062
Vegetation Type	Croplands	Mixed forests	Evergreen needleleaf forests	Evergreen broadleaf forests	Evergreen broadleaf forests	Grasslands	Grasslands	Grasslands

to a relatively high LUE of shaded leaves under cloudy and aerosol-laden skies (Zhou et al. 2016). Considering the different abilities of PAR absorption and LUE of sunlit and shaded leaves, He et al. (2013) proposed a two-leaf light use efficiency model (TL-LUE) by calculating the LUE and GPP of sunlit and shaded leaves separately. This algorithm was proven to have better performance for GPP estimation than a one-leaf model.

However, the accuracy of RS-based LUE models varies with climate factors, input data, parameters, and biome types (Chen et al. 2014; Liu et al. 2014; Turner et al. 2006; Yuan et al. 2014). Numerous sensitivity studies have been conducted to evaluate the impact of the aforementioned factors on GPP estimation. Turner et al. (2006) investigated Moderate Resolution Imaging Spectroradiometer (MODIS) GPP estimates of different biome types and found overestimation for low productivity area and underestimation for high productivity area. Yuan et al. (2014) found that seven RS-based LUE models exhibited underestimation under cloudy sky conditions and showed various performances for different biome types. Xie et al. (2019) assessed the uncertainties in GPP estimations caused by different leaf area index (LAI) datasets. Sun et al. (2019) evaluated the sensitivity of GPP estimations from 14 models to CO₂ concentrations based on remote sensing data. A variety of studies have also investigated GPP model accuracy with respect to climate factors, including drought (Stocker et al. 2019; Wagle et al. 2014), sky clearness (He et al. 2013; Wang et al. 2015), temperature, precipitation and radiation (Sabetaftar et al. 2011; Sun et al. 2019).

These studies emphasize the necessity to evaluate and understand the sensitivity of GPP estimation models to the influencing factors before designing and improving the models (Liu et al. 2014; Sun et al. 2019). The diffuse radiation fertilization effect of PAR_{dif} can enhance the photosynthesis of shaded leaves, which cannot be neglected in GPP estimation (Cohan et al. 2002; Rap et al. 2018). Given the total PAR, a larger PAR_{dif} fraction will lead to more diffuse PAR than direct PAR, which will consequently affect the GPP estimation. However, the sensitivity of a LUE model to the fraction of PAR_{dif} is still not comprehensively understood. The impact of various PAR_{dif} fraction levels on the GPP estimation accuracy is unclear. Additionally, as one of the main factors influencing PAR_{dif} on clear days (Dong et al. 2016), aerosols are believed to decrease PAR_{dir} and increase PAR_{dif} by scattering and absorption, which indirectly affect the photosynthesis and production of plants (Li et al. 2020). Substantial efforts have been made to explore the relationship between aerosols and plant production in various ecosystems and regions using observed or simulated data (Cohan et al. 2002; Kumar and Kumar 2017; Strada et al. 2015). Nevertheless, studies related to the impact of aerosols on GPP estimation are still limited.

To extend the understanding of the sensitivity of GPP estimations to the PAR_{dif} fraction and aerosols, this paper evaluates the responses of one-leaf and two-leaf models (MOD17 and TL-LUE) to the variations in the PAR_{dif} fraction (the ratio of PAR_{dif} in PAR_{total}) and aerosol loading by using MODIS data and flux tower observations of ChinaFLUX. In addition, to investigate the errors of the calculated changes in GPP with the

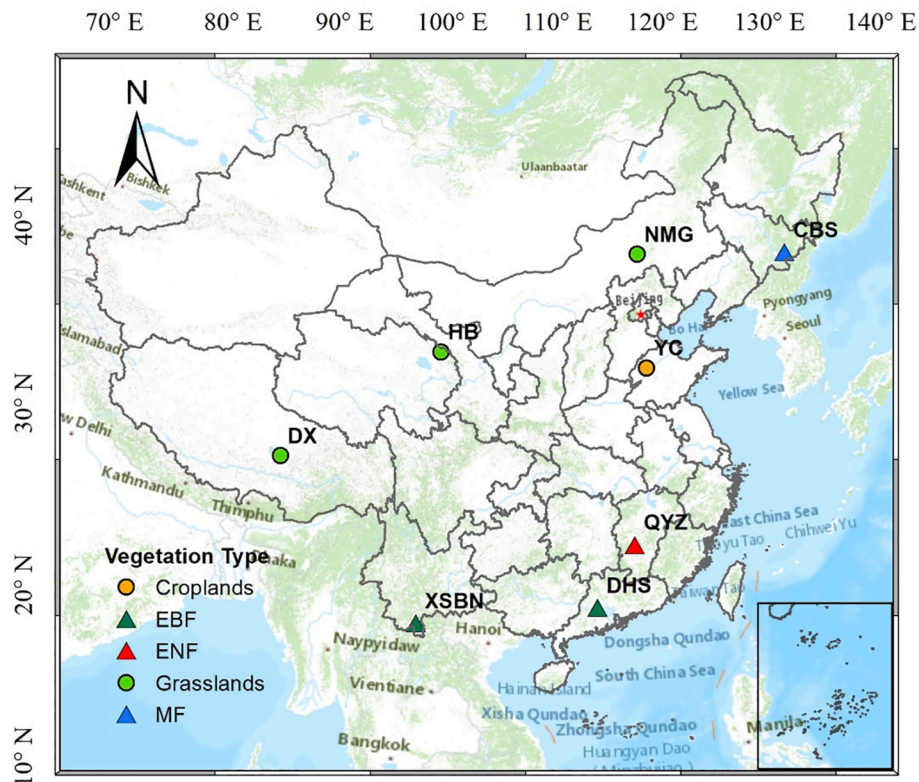


Fig. 1. Spatial distribution of the eight ChinaFLUX sites including cropland site (YC), mixed forest (MF) site (CBS), evergreen needleleaf forest (ENF) site (QYZ), evergreen broadleaf forest (EBF) sites (DHS and XSBN), and grassland sites (HB, NMG and DX).

variations in the two factors, the accuracies of the two models are compared with the changes in the PAR_{dif} fraction and aerosol optical depth (AOD, a unitless measurement of aerosol loading) to assess the impacts of the PAR_{dif} fraction and AOD change on model performance.

2. Data

2.1. MODIS data

The MOD15A2, MCD43A3, and MOD08_E3 products from 2003 to 2010 were used in this study. All MODIS products were obtained from NASA Level-1 and the Atmosphere Archive & Distribution System Distributed Active Archive Center (DAAC) (<https://ladsweb.modaps.eosdis.nasa.gov/search/>). The eight-day composite MOD15A2 product was used to obtain LAI and fraction of PAR absorbed by vegetation (fPAR) data at 500 m resolution. To remain consistent with the footprint of the flux tower, the LAI and fPAR values at each site were derived from the mean values of pixels located within 3 km from the center of the site (Zhou et al. 2016). The LAI and fPAR time series were filtered using quality flags (QA) in MOD15A2 products to exclude cloud contaminated pixels. The locally adjusted cubic-spline capping (LACC) method (Chen et al. 2006) was applied to reconstruct the fPAR and LAI time series by filling the masked values and smoothing abnormal values due to the residual effect of atmosphere and cloud contamination (Zan et al. 2018). The time series of fPAR and LAI during 2003–2010 before and after LACC smoothing are shown in Figure S1 and S2. The fPAR and LAI values affected by atmospheric corrections or other artifacts are replaced by the values calculated by the LACC method, which has been proven to be a quality control for LAI and fPAR time series (Chen et al. 2006).

The albedo data of the 500-m grid were derived from the MODIS daily black-sky albedo product (MCD43A3) and averaged over eight-day time intervals to remain consistent with the temporal resolution of the MOD15A2 data. The albedo at each site was also averaged based on the values of pixels located within 3 km from the center of the site. The albedo time series was also filtered by the QA field and smoothed by LACC.

The MODIS C6 level-3 products (MOD08_E3) with 1° resolution were used to obtain the eight-day combined Deep Blue and Dark Target (DB/DT) AOD data. The AOD at each site was the value of the pixel that overlapped the target site. Due to the cloud contamination and the presence of ground snow and ice, the AOD data were masked by quality flags. The LACC was used to fill the missing or contaminated values in the AOD time series.

2.2. Flux data

The flux measurements at eight sites across China, including the daily ecosystem respiration (RE), net ecosystem exchange (NEE), and meteorological data were downloaded from the ChinaFLUX database (<http://rs.cern.ac.cn/index.jsp>). The ChinaFLUX NEE data were measured directly by the eddy-flux technique, while the RE data at all sites were calculated using the Lloyd–Taylor equation (Lloyd and Taylor 1994; Wang et al. 2015; Zhu et al. 2020). The eight sites include one cropland site (YC), three grassland sites (HB, NMG and DX), and four forest sites (CBS, QYZ, DHS and XSNB). The vegetation types and locations of these sites are shown in Table 1 and Fig. 1. The observation period spanned from January 2003 to December 2010. Since the GPP cannot be measured directly, the GPP at each site was derived from the difference in the observed RE and NEE ($GPP = RE - NEE$) (Liu et al. 2014; Strada et al. 2015). The GPP derived from the ChinaFLUX measurements (GPP_FLUX) was used to calibrate model parameters and validate the MOD17 and TL-LUE models. In addition, daily meteorological measurements, including air temperature (Ta) and vapor pressure deficit (VPD), at the ChinaFLUX sites were also employed in the LUE model. To remain consistent with the temporal resolution of the MODIS eight-day

Table 2
Parameters of the MOD17 model for different vegetation types.

Vegetation Type	ENF	EBF	MF	Grasslands	Croplands
ϵ_{max} (g CMJ ⁻¹)	0.962	1.268	1.051	0.860	1.044
T_{amin_min} (°C)	−8	−8	−7	−8	−8
T_{amin_max} (°C)	8.31	9.09	9.5	12.02	12.02
VPD_{min} (kPa)	6.5	8	6.5	6.5	6.5
VPD_{max} (kPa)	46	31	24	53	43
Ω	0.6	0.8	0.7	0.9	0.9

ENF is evergreen needleleaf forests; EBF is evergreen broadleaf forests; MF is mixed forests

products, the daily GPP_FLUX and meteorological measurements were averaged over an eight-day time interval.

2.3. CERES data

The daily PAR data at a 1° × 1° latitude–longitude grid, including the direct and diffuse composition (PAR_{dir} and PAR_{dif}), were derived from the Clouds and the Earth's Radiant Energy System (CERES) SYN1deg edition 4.1 product, which were obtained from the project website (<https://ceres-tool.larc.nasa.gov/ord-tool/jsp/SYN1degEd41Selection.jsp>). The total PAR (PAR_{total}) is composed of PAR_{dir} and PAR_{dif} . The CERES data were validated by daily PAR_{dir} and PAR_{dif} observations at six sites (Table S1) obtained from China Meteorological Data Service Center (CMDC, <http://data.cma.cn/>) during 2004–2010. As shown in Figure S3, the CERES PAR has a good agreement with observations from the CMDC with a slope around 0.9 and R² larger than 0.8. The PAR_{dir} and PAR_{dif} RMSEs are 1.35 MJ m⁻² d⁻¹ and 0.9835 MJ m⁻² d⁻¹, respectively. The daily PAR_{dir} and PAR_{dif} data were averaged to an eight-day temporal resolution corresponding to the MODIS products. The PAR at each site was the pixel value corresponding to the target site.

3. Methodology

3.1. MOD17 model

The MOD17 model (Running et al. 2000) was developed from the radiation conversion efficiency theory of Monteith (1972) and calculated GPP as follows:

$$GPP = \epsilon_{max} \times g(T_{amin}) \times f(VPD) \times PAR_{total} \times fPAR \quad (1)$$

where ϵ_{max} is the maximum LUE, with the default value shown in Table 2; $g(T_{amin})$ and $f(VPD)$ are the scalars of the minimum air temperature and VPD, respectively, which vary from in the range of [0, 1] and downscale the ϵ_{max} to the real LUE; PAR_{total} is the total incident PAR; and fPAR is the fraction of PAR absorbed by the whole canopy. The term $PAR_{total} \times fPAR$ represents the absorbed PAR for vegetation (APAR). The VPD and T_{amin} scalars in Eq. (1) are calculated as follows:

$$f(VPD) = \begin{cases} 0 & VPD \geq VPD_{max} \\ \frac{VPD_{max} - VPD}{VPD_{max} - VPD_{min}} & VPD_{min} < VPD < VPD_{max} \\ 1 & VPD \leq VPD_{min} \end{cases} \quad (2)$$

$$g(T_{amin}) = \begin{cases} 0 & T_{amin} \leq T_{aminmin} \\ \frac{T_{amin} - T_{aminmin}}{T_{aminmax} - T_{aminmin}} & T_{aminmin} < T_{amin} < T_{aminmax} \\ 1 & T_{amin} \geq T_{aminmax} \end{cases} \quad (3)$$

where VPD and T_{amin} are daily measurements of average VPD and minimum air temperature, respectively; VPD_{max} and VPD_{min} are daily average VPD for maximum (ϵ_{max}) and minimum (0) LUE, respectively; $T_{aminmin}$ and $T_{aminmax}$ represents the daily minimum temperature for

Table 3
Calibrated model parameters of ϵ_{max} , ϵ_{sun} , and ϵ_{sh} for eight ChinaFLUX sites.

Sites	YC	CBS	QYZ	DHS	XSBN	HB	NMG	DX
$\epsilon_{max}(\text{gCM J}^{-1})$	1.661	1.007	0.821	0.591	0.961	0.747	0.632	0.176
$\epsilon_{sun}(\text{gCM J}^{-1})$	1.336	0.931	0.758	0.336	0.551	0.646	0.587	0.105
$\epsilon_{sh}(\text{gCM J}^{-1})$	2.420	1.341	1.023	0.861	1.682	1.081	1.140	0.293

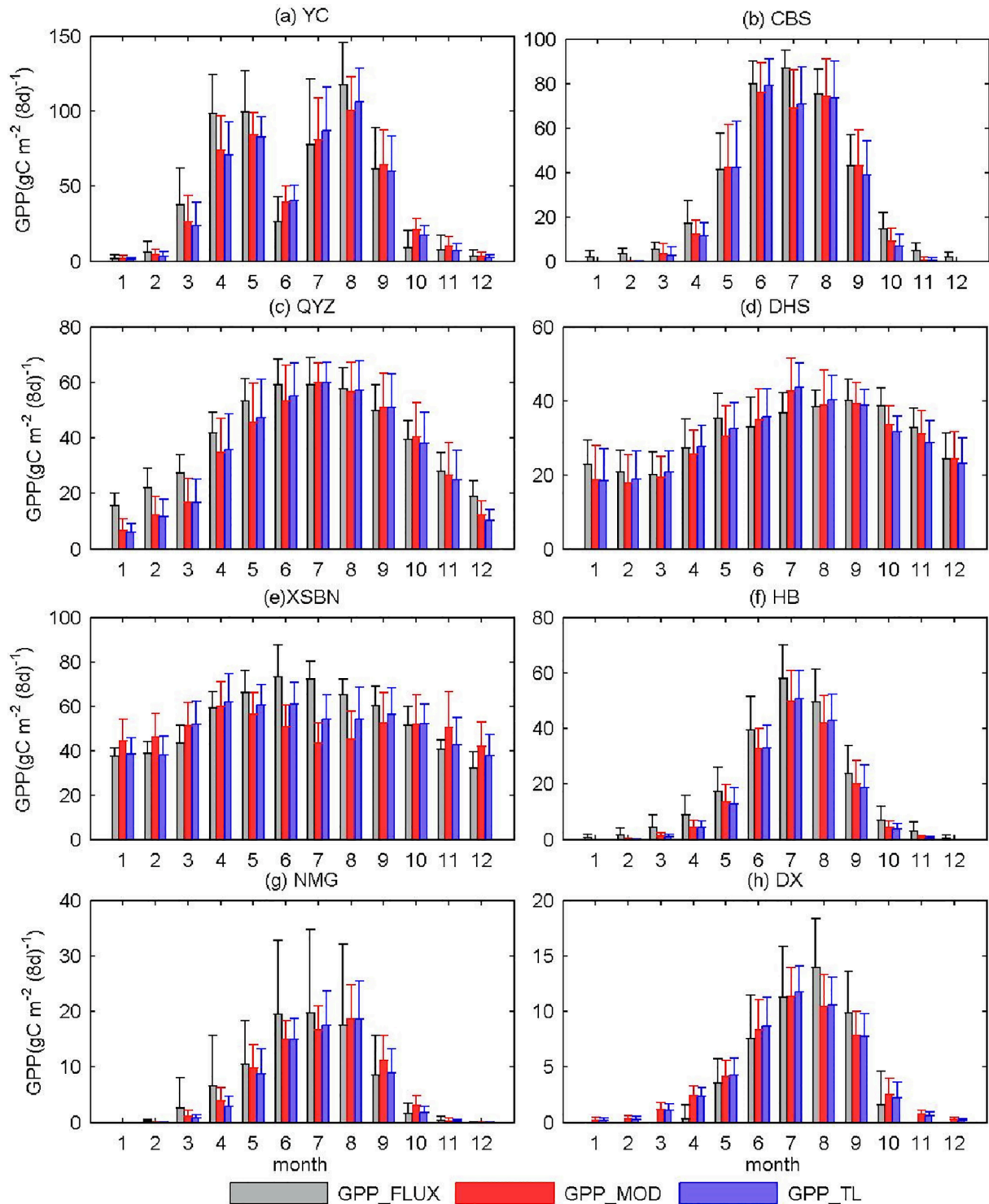


Fig. 2. Seasonal variations in eight-day observed GPP (GPP_FLUX) and estimated GPP (GPP_MOD and GPP_LUE) from the MOD17 and TL-LUE models at the eight ChinaFLUX sites during 2001–2010.

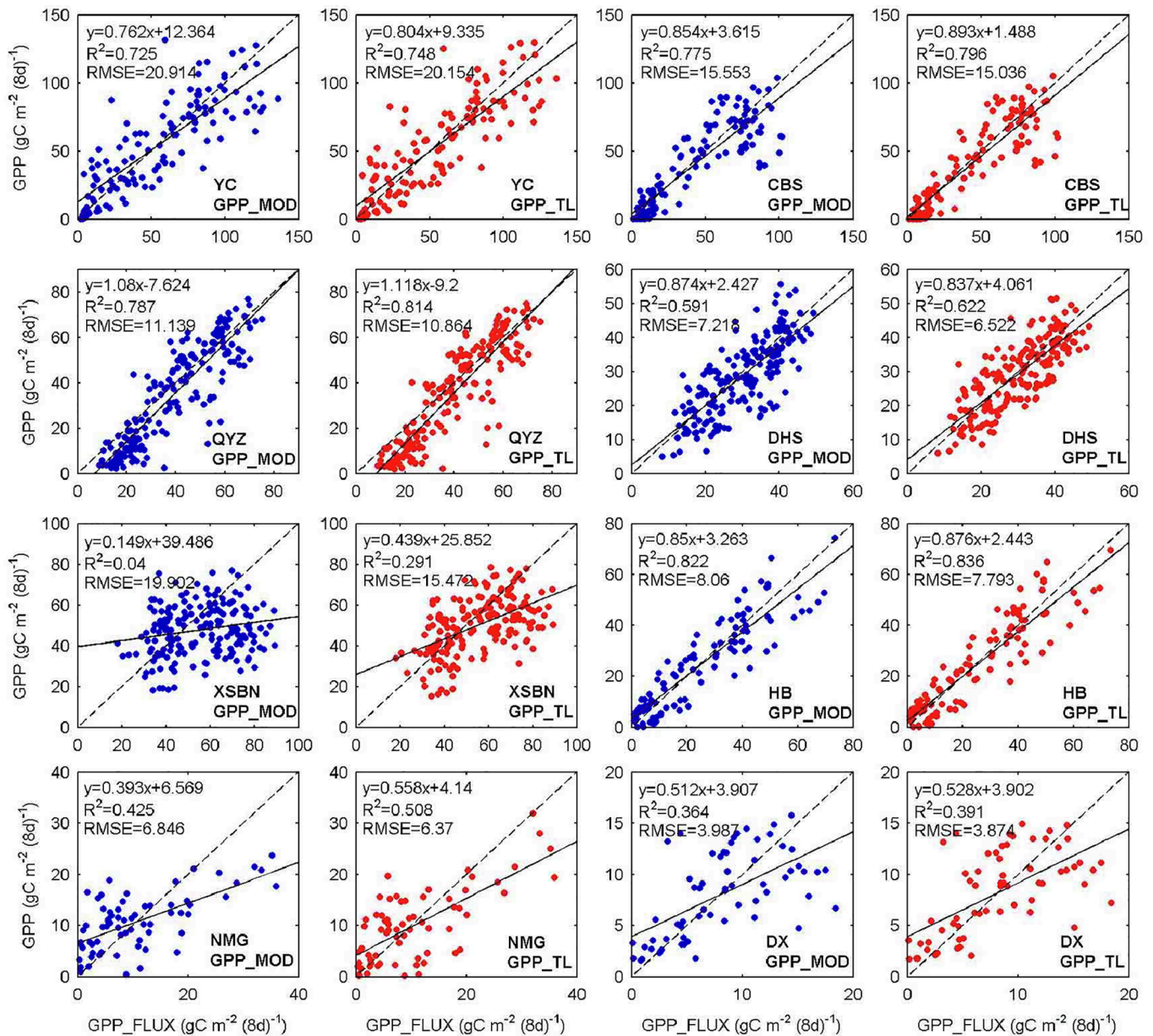


Fig. 3. Scatterplots between the estimated eight-day GPP (GPP_MOD and GPP_TL) using MOD17 and TL-LUE models and the measured GPP by ChinaFLUX (GPP_FLUX) in calibration years from 2003 to 2006. The blue dots GPP_MOD against GPP_FLUX while the red dots are GPP_TL against GPP_FLUX. The solid line is the regression line while the dashed line is the one-one line. (For interpretation of the references to colour in this figure legend, the reader is referred to the web version of this article.)

maximum and minimum LUE; VPD_{max} , VPD_{min} , $T_{aminmin}$ and $T_{aminmax}$ are parameters derived from Biome Properties Look-Up Table (BPLUT), and they vary with the vegetation types, as shown in Table 2 (Running et al. 2015).

3.2. TL-LUE model

The TL-LUE model was developed based on the MOD17 and boreal ecosystem productivity simulator (BEPs) models by separating the canopy into sunlit and shaded leaf groups (He et al. 2013). The GPP is calculated as follows:

$$GPP = (\epsilon_{msu} \times APAP_{su} + \epsilon_{msh} \times APAP_{sh}) \times f(VPD) \times g(T_{amin}) \quad (4)$$

where ϵ_{msu} and ϵ_{msh} are the maximum LUE of sunlit and shaded leaves, respectively; and $APAP_{su}$ and $APAP_{sh}$ are the absorbed PAR of the sunlit

and shaded leaves, which are defined as:

$$APAP_{su} = (1 - \alpha) \times [PAR_{dir} \times \frac{\cos(\beta)}{\cos(\theta)} + \frac{PAR_{dif} - PAR_{dif,u}}{LAI} + C] \times LAI_{su} \quad (5)$$

$$APAP_{sh} = (1 - \alpha) \times [\frac{PAR_{dif} - PAR_{dif,u}}{LAI} + C] \times LAI_{sh} \quad (6)$$

where α is the albedo relative to vegetation cover; PAR_{dir} and PAR_{dif} are the direct and diffuse components of PAR, respectively; β is the mean leaf-sun angle and is set as 60° for a canopy with spherical leaf angle distribution (Chen et al. 1999); θ is the solar zenith; LAI is the total leaf area index of the canopy; $\frac{PAR_{dif} - PAR_{dif,u}}{LAI}$ depicts the PAR_{dif} per unit leaf area for the canopy; $PAR_{dif,u}$ is the diffuse radiation under the plant canopy; and C represents the contribution of multiple scattering of the PAR_{total} to the PAR_{dif} . LAI_{su} and LAI_{sh} are the LAI of sunlit and shaded leaves,

Table 4
Comparison of R^2 and RMSE of the GPP_MOD and GPP_TL for calibration and validation years.

Site	GPP_MOD		GPP_TL		Difference	
	R^2	RMSE (gCm ⁻² (8d) ⁻¹)	R^2	RMSE (gCm ⁻² (8d) ⁻¹)	ΔR^2	Δ RMSE (gCm ⁻² (8d) ⁻¹)
Calibration Years						
YC	0.725	20.914	0.748	20.154	0.023	-0.760
CBS	0.775	15.553	0.796	15.036	0.021	-0.517
QYZ	0.787	11.139	0.814	10.864	0.027	-0.275
DHS	0.591	7.218	0.622	6.522	0.031	-0.696
XSBN	0.040	19.902	0.291	15.472	0.251	-4.430
HB	0.822	8.060	0.836	7.793	0.014	-0.267
NMG	0.425	6.846	0.508	6.370	0.083	-0.476
DX	0.364	3.987	0.391	3.874	0.027	-0.113
Validation Years						
YC	0.843	22.54	0.839	22.225	0.004	-0.315
CBS	0.817	14.999	0.837	14.66	0.020	-0.339
QYZ	0.837	10.024	0.848	9.821	0.011	-0.203
DHS	0.521	8.027	0.556	7.426	0.035	-0.601
XSBN	0.025	18.525	0.336	13.684	0.311	-4.841
HB	0.958	10.971	0.964	10.809	0.006	-0.162
NMG	0.435	10.333	0.467	10.032	0.032	-0.301
DX	0.203	5.120	0.223	5.002	0.020	-0.118

ΔR^2 equals R^2 of GPP_TL minus that of GPP_MOD; RMSE is RMSE of GPP_TL minus that of GPP_MOD.

respectively.

$$LAI_{su} = 2\cos(\theta)(1 - \exp(-0.5\Omega \frac{LAI}{\cos(\theta)})) \quad (7)$$

$$LAI_{sh} = LAI - LAI_{su} \quad (8)$$

where Ω represents the clumping index depending on the spatial distribution of vegetation foliage (Table 2). A smaller Ω value indicates larger foliage clumping, allowing more radiation to penetrate through the canopy (Chen et al. 1999).

The $PAR_{dif,u}$ and C in Eqs. (5) and (6) are computed following the study of Chen et al. (1999).

$$PAR_{dif,u} = PAR_{dif} \exp(-0.5\Omega LAI / (0.537 + 0.025LAI)) \quad (9)$$

$$C = 0.07\Omega PAR_{dir} (1.1 - 0.1LAI) \exp(-\cos\theta) \quad (10)$$

3.3. Model calibration and validation

To reduce the GPP estimation bias caused by the maximum LUE, the optimized values of parameters ϵ_{max} , ϵ_{sun} and ϵ_{sh} in the MOD17 and TL-LUE models were calibrated using linear least-square regression to minimize the root-mean-square error (RMSE) between the estimated and measured eight-day GPP at the ChinaFLUX sites during 2003–2006. The GPP measurements from ChinaFLUX from 2007 to 2010 were employed to validate the GPP estimations from the two models. A linear regression was performed between the estimated and measured GPP, and the coefficient of determination (R^2) and RMSE were calculated to assess the performance of the two models in the calibration and validation procedures.

4. Results and discussion

4.1. Calibrated model parameters

Table 3 lists the calibrated ϵ_{max} from the MOD17 model and ϵ_{sun} and ϵ_{sh} from the TL-LUE model at the eight China-FLUX sites. These calibrated parameters vary substantially in space. Although the HB, NMG and DX sites are covered by the same vegetation type, their ϵ_{max} , ϵ_{sun} and ϵ_{sh} values are different. This difference is because in addition to the vegetation cover, the forest canopy architecture, plant species and leaf element contents can also lead to the dynamic maximum LUE (Zhou et al. 2016). The calibrated ϵ_{sun} ranges from 0.167 (DX) to 1.318 (YC), while the calibrated ϵ_{sh} ranges from 0.191 (DX) to 2.445 (YC). The

parameters at the YC cropland site are higher than those at other sites in forests or grasslands, which may be caused by artificial fertilization and high water use efficiencies (Zhou et al. 2016). The calibrated ϵ_{sh} is 1.2–1.8 times larger than the calibrated ϵ_{max} , while the calibrated ϵ_{sun} is 7.1%–43.1% lower than the calibrated ϵ_{max} , indicating that shaded leaves have higher LUE than sunlit leaves.

4.2. Comparison of model performance

As shown in Fig. 2, the seasonal variations in the estimated GPP from the MOD17 and TL_LUE models (GPP_MOD and GPP_TL) are consistent with the GPP_FLUX measured at eight sites. For most sites, GPP is highest from June to August, corresponding with the peak of plant growth. The crops at the YC site have two peaks of GPP in spring and summer, which corresponds to winter wheat and summer maize rotations (He et al. 2013).

Fig. 3 compares GPP_MOD and GPP_TL with GPP_FLUX at the eight ChinaFLUX sites for the calibration years (2003–2006). The performances of the two models differ substantially at different sites. Both GPP_MOD and GPP_TL have good agreement with GPP_FLUX at the YC, CBS, QYZ, and HB sites with $R^2 > 0.7$. The coefficient of determination (R^2) for GPP_MOD ranges from 0.04 at XSBN to 0.82 at HB. The RMSE between GPP_MOD and GPP_FLUX is smallest at DX (3.987 gCm⁻²(8 d)⁻¹) and largest at YC (20.914 gCm⁻²(8 d)⁻¹). The GPP_TL has better agreement with GPP_FLUX than GPP_MOD with higher R^2 (0.291–0.836) and smaller RMSE (3.874–20.154) values at all sites. GPP_TL has the best agreement with GPP_FLUX at HB, with an R^2 of 0.836. The enhancement of GPP_TL compared with GPP_MOD is most significant at XSBN, with R^2 increasing from 0.04 to 0.291 and RMSE decreasing from 19.902 gCm⁻²(8d)⁻¹ to 15.472 gCm⁻²(8d)⁻¹ (Table 4).

The eight-day composite GPP of the two models during 2007–2010 are calculated using the optimized parameters and validated with GPP_FLUX at the eight sites (Fig. 4). During the validation years, GPP_TL outperforms GPP_MOD with a higher R^2 and smaller RMSE. Both GPP_MOD and GPP_TL have the highest R^2 values (0.958 and 0.964) at the HB site. The accuracy of GPP_TL exhibits the largest improvement at XSBN with the largest R^2 increase and RMSE decrease compared with that of GPP_MOD in both calibration and validation years (Table 4). In both Fig. 3 and Fig. 4, the regression line of the estimated GPP and GPP_FLUX is generally below the one–one line for all sites, indicating that both the MOD17 and TL-LUE models underestimate GPP. The regression line of GPP_TL is closer to the one–one line than GPP_MOD, suggesting that the underestimation of GPP_TL is less than that of

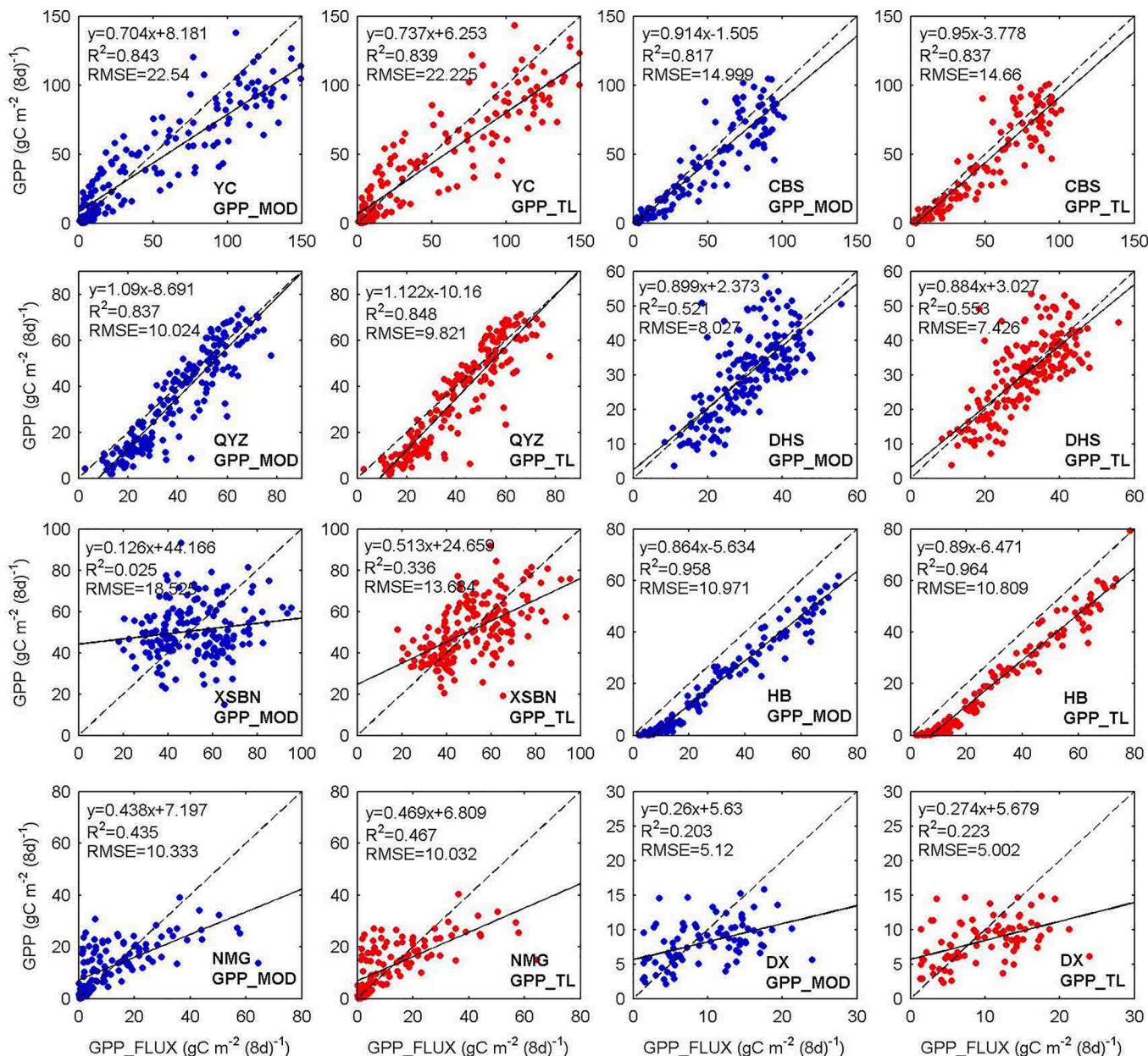


Fig. 4. Scatterplots between the estimated eight-day GPP (GPP_MOD and GPP_TL) using the MOD17 and TL-LUE models and the measured GPP by ChinaFLUX (GPP_FLUX) in the validation years from 2007 to 2010.

GPP_MOD, which is obvious at the YC, CBS, XSBN and NMG sites.

4.3. Sensitivity of the estimated GPP to the PAR_{dif} fraction

The sensitivity of the estimated GPP to the PAR_{dif} fraction was assessed by calculating the bias and RMSE between the estimated GPP and GPP_FLUX at different PAR_{dif} fraction ranges. Fig. 5 shows the trend of the bias between the estimated GPP (GPP_MOD and GPP_TL) and GPP_FLUX with varied PAR_{dif} fractions. The GPP_MOD is systematically underestimated compared with GPP_FLUX when the PAR_{dif} fraction is high, and the degree of underestimation increases as the PAR_{dif} fraction increases. The GPP_MOD is overestimated when the PAR_{dif} fraction is low at the YC, CBS, DHS, XSBN and DX sites. The GPP_TL generally shows a consistent trend with GPP_MOD but the underestimation decreases when the PAR_{dif} fraction is larger than 0.8 for most sites, indicating that the TL-LUE model mitigates the sensitivity of the estimated GPP to the PAR_{dif} fraction. This result occurs because when the PAR_{dif}

fraction increases, the APAR of shaded leaves increases. Furthermore, ϵ_{sh} has a larger value than both ϵ_{max} and ϵ_{sun} ; therefore, GPP_TL is larger than GPP_MOD and exhibits a smaller deviation from GPP_FLUX. The TL_LUE model also decreases the overestimation at low PAR_{dif} fractions (<0.6) at evergreen broadleaf forest sites (DHS and XSBN). However, the TL_LUE model leads to a larger underestimation than MOD17 for the cropland, grassland and evergreen needleleaf forest sites when the PAR_{dif} fraction is low. The reason for this finding is that the APAR of sunlit leaves dominates the whole canopy when the PAR_{dif} fraction is low. Additionally, ϵ_{sun} is lower than both ϵ_{sh} and ϵ_{max} ; thus, GPP_TL is lower than GPP_MOD. Therefore, GPP_TL exhibits less overestimation when GPP_MOD overestimates at low PAR_{dif} fraction and exhibits greater underestimation when GPP_MOD underestimates the values and PAR_{dif} fraction is low.

As shown in Fig. 6, the RMSE of GPP_MOD and GPP_TL shows an upward trend as the PAR_{dif} fraction increases at the YC, CBS, QYZ, HB, and DX sites. The GPP_MOD and GPP_TL RMSE values are high at the

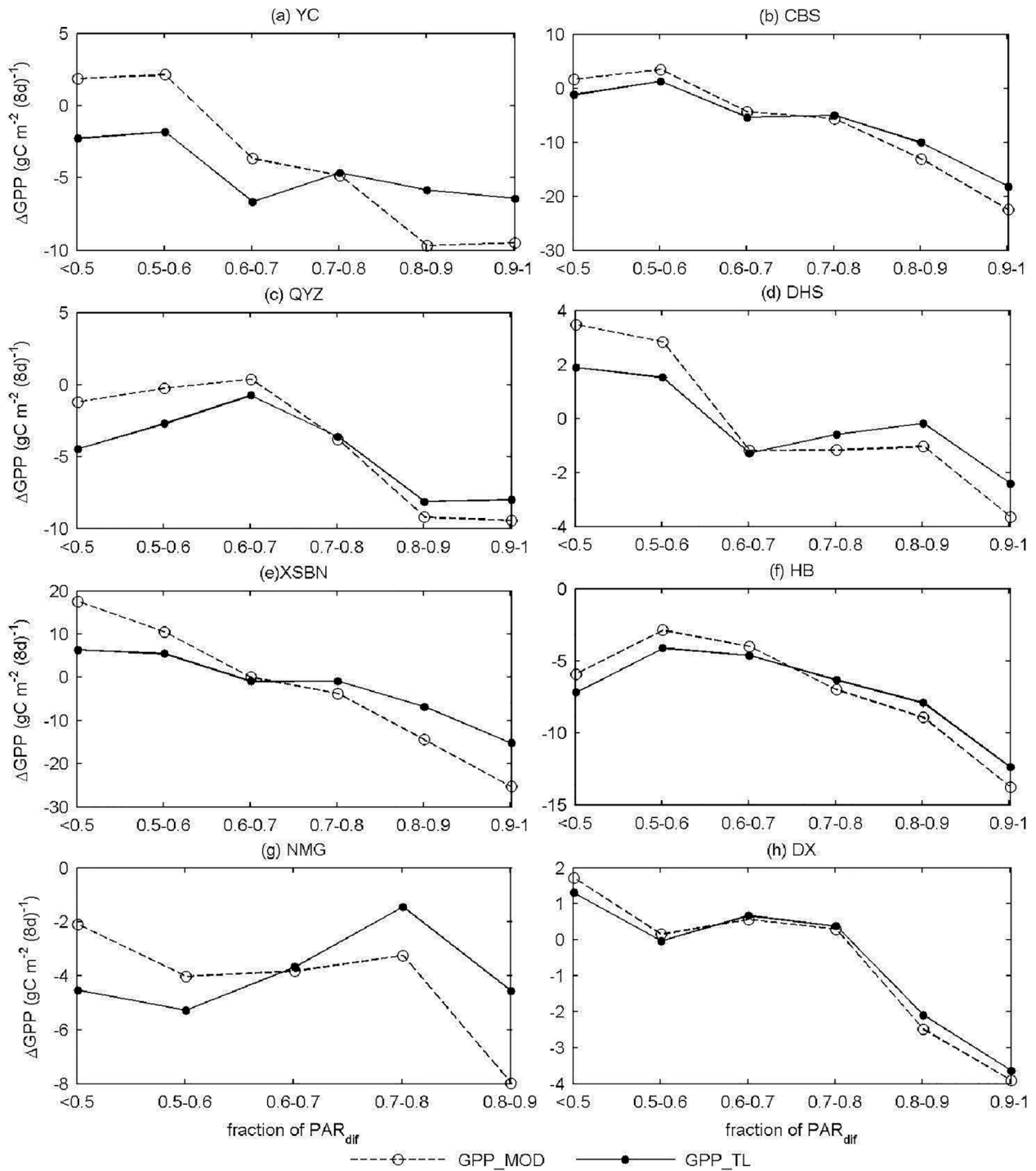


Fig. 5. Averaged bias between the estimated GPP from two models (GPP_{MOD} and GPP_{TL}) using calibrated parameters and the measured GPP at ChinaFLUX sites during 2003–2010 with fraction of PAR_{dif} . (ΔGPP equals estimated GPP minus measured GPP).

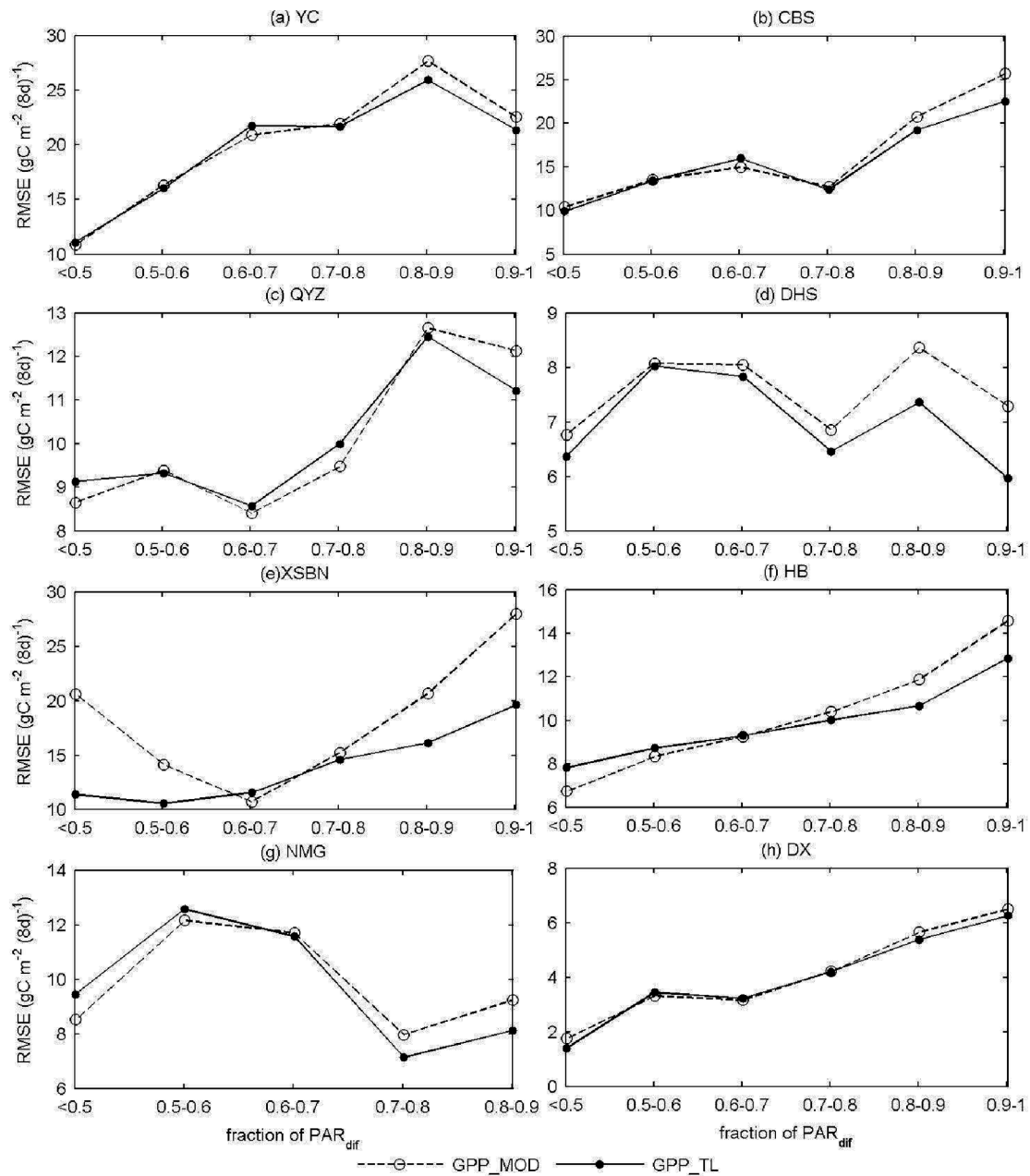


Fig. 6. RMSE between the estimated GPP from two models (GPP_MOD and GPP_TL) using calibrated parameters and the measured GPP at ChinaFLUX sites during 2003–2010 with fraction of PAR_{dif} .

DHS and NMG sites when PAR_{dif} is low, possibly due to large overestimation of the low PAR_{dif} fraction. A comparison of bias and the RMSE of GPP_MOD and GPP_TL shows that the TL_LUE model starts to outperform the MOD17 model when the PAR_{dif} fraction is above 0.7 or 0.8 for most sites. For the evergreen needleleaf forest sites, the TL_LUE model also has better accuracy than the MOD17 model, with a small RMSE for the low PAR_{dif} fraction. However, for the other sites, GPP_TL has a larger RMSE than GPP_MOD for low PAR_{dif} (<math><0.7</math>), which is a result of the greater underestimation of GPP_TL compared with GPP_MOD (Fig. 6). Both GPP_TL and GPP_MOD show the largest RMSE at the crop site (YC) when the PAR_{dif} fraction is high (>math>0.8</math>). The DX site has the smallest RMSE for all PAR_{dif} fraction ranges, which is consistent with the result in Fig. 4. Relative to MOD17, TL_LUE shows the greatest improvement in terms of bias and RMSE at the XSBN site, which is covered by tropical rainforests. This is because the diffuse PAR is higher

in tropical rainforests than in other biome types (Yan et al. 2017), which leads to a larger impact of the PAR_{dif} fraction on GPP estimation.

To illustrate how the LUE varies with the PAR_{dif} fraction, the observed LUE ($\text{LUE} = \text{GPP}_{\text{FLUX}}/\text{PAR}$) and simulated LUE ($\text{LUE} = \text{GPP}_{\text{MOD}}/\text{PAR}$ and $\text{LUE} = \text{GPP}_{\text{TL}}/\text{PAR}$) in different PAR_{dif} fraction ranges were calculated (Fig. 7). The observed LUE generally shows a rising trend with the increasing PAR_{dif} fraction at all sites, implying the positive impact of PAR_{dif} on LUE. The simulated LUE by the TL_LUE model shows a similar pattern to the observed LUE while the LUE of the MOD17 model does not increase with the increase in the PAR_{dif} fraction at the evergreen broadleaf forest sites (DHS and XSBN). In general, the LUE of GPP_MOD is higher than that of GPP_TL at the low PAR_{dif} fraction. Both the TL_LUE and MOD17 models tend to underestimate the LUE when the PAR_{dif} fraction is larger than 0.7. For the evergreen broadleaf forest sites, the two models have overestimation at low PAR_{dif}

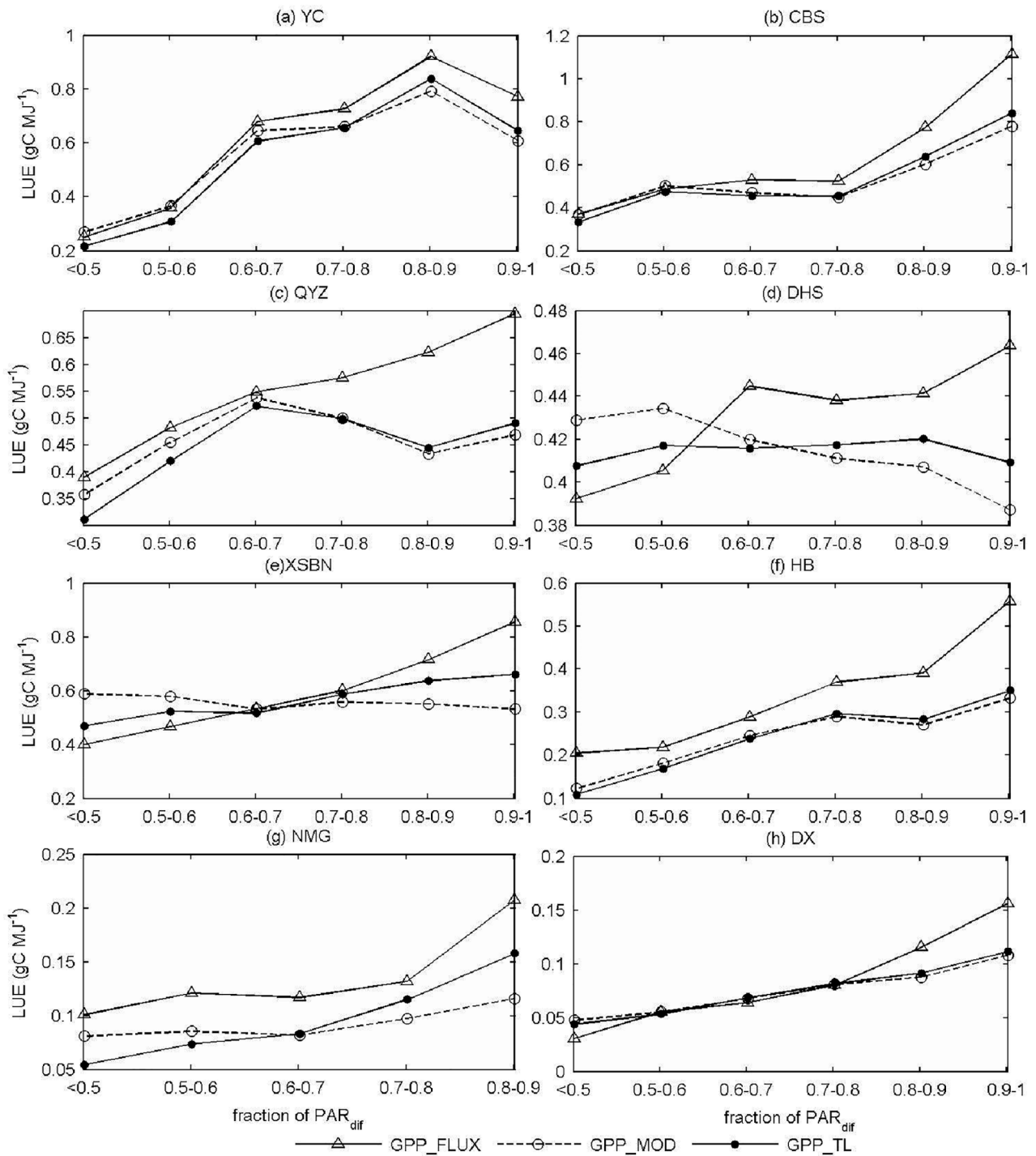


Fig. 7. Dependence of the observed and modelled light use efficiency (LUE) on the fraction of PAR_{dif} in validation years.

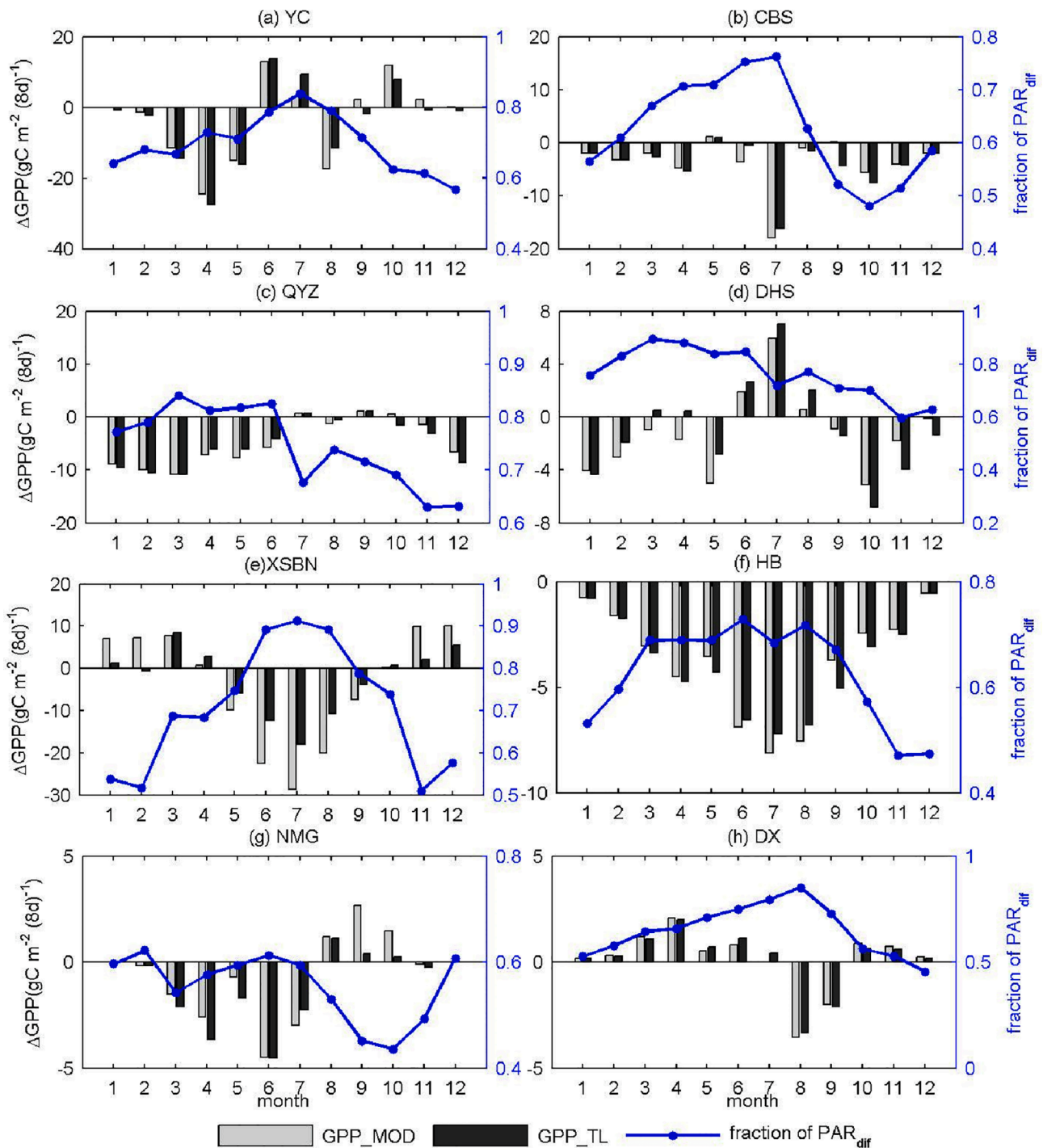


Fig. 8. Seasonal variation in the averaged bias between the estimated GPP (GPP_MOD and GPP_TL) and the measured GPP at China Flux sites and the averaged fraction of PAR_{dif} during 2003–2010.

fraction (<0.6). In addition, the LUE overestimation of GPP_TL is lower than that of GPP_MOD at the low PAR_{dif} fraction.

To explore the seasonal variations in the estimated GPP sensitivity to the PAR_{dif} fraction, the bias between the estimated and measured GPP is calculated in each month. As shown by the blue line in Fig. 8, the fraction of PAR_{dif} exhibits different seasonal variations at different sites. Specifically, the PAR_{dif} fraction reaches its peak in summer (June to August) at the YC, CBS, XSBN, and DX sites, while the PAR_{dif} fraction at QYZ and DHS has higher values in spring (March to May) than in other seasons. Although the trend of the PAR_{dif} fraction varies, both the MOD17 and TL_LUE models produce larger underestimations of GPP in

the months with high PAR_{dif} fractions than in those with low PAR_{dif} fractions at most sites except YC. The estimated GPP in YC is also underestimated in April and May when the winter wheat reaches the growth peak with a high GPP value. For most sites, the GPP_TL has less underestimation than GPP_MOD in the months with high PAR_{dif} fractions, which is most obvious at the forest sites (QYZ, CBS, DHS, and XSBN).

4.4. The sensitivity of the estimated GPP to AOD

Different sites exhibit various AOD levels, with the highest levels

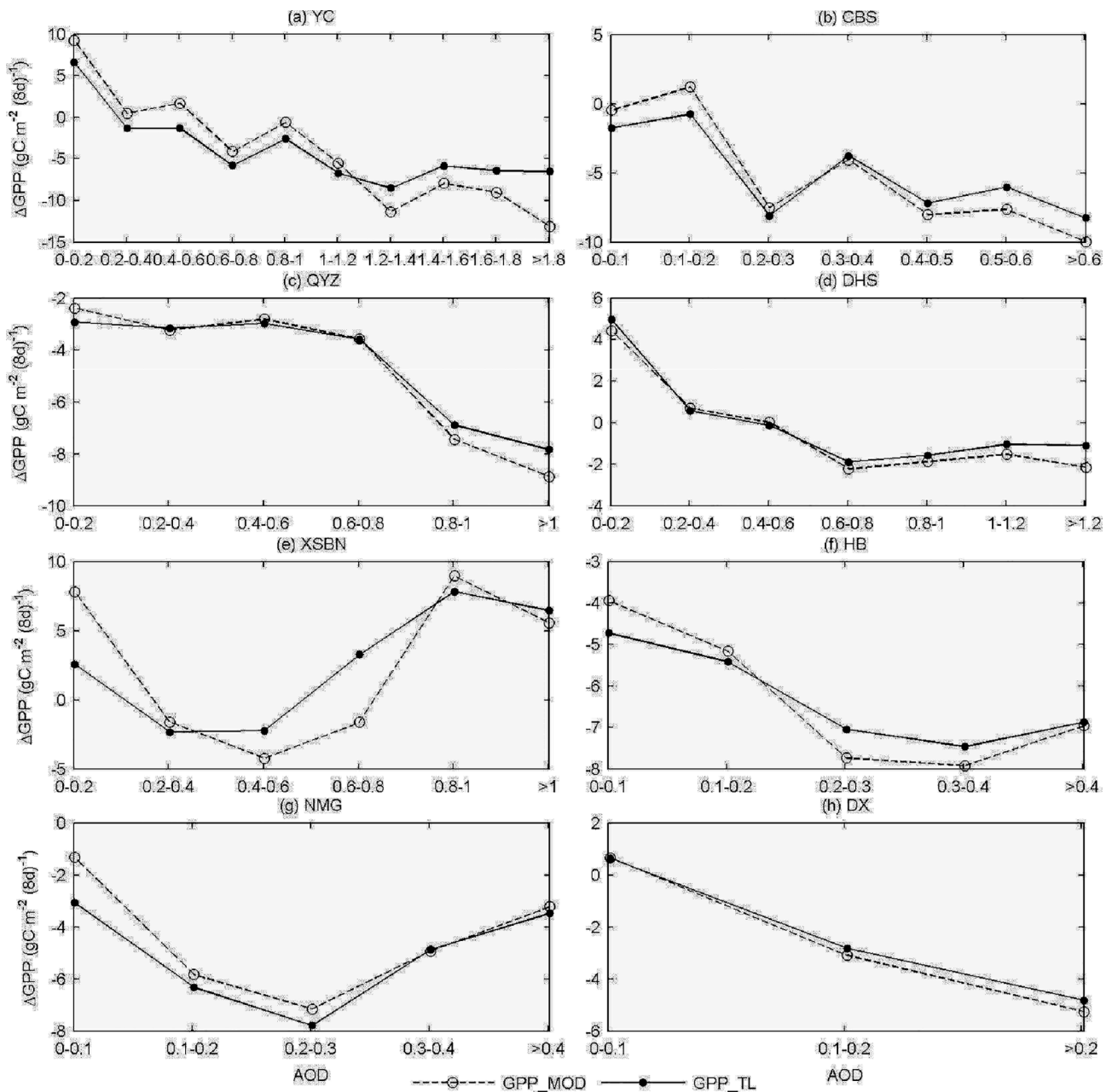


Fig. 9. Averaged bias between the estimated GPP from two models (MOD17 and TL-LUE) using calibrated parameters and the measured GPP at the ChinaFLUX sites from 2003 to 2010 with the AOD changes. (Δ GPP equals estimated GPP minus measured GPP).

observed in YC and lowest levels observed in DX. As shown in Fig. 9, the ChinaFLUX sites with different aerosol loadings and land covers have inconsistent GPP estimation errors. The YC site has the largest underestimation (larger than $10 \text{ gCm}^{-2}(8\text{d})^{-1}$) for high AOD values. GPP overestimation occurs when AOD is low at the YC, CBS, DHS, XSBN, and DX sites, which coincides with the sites having overestimation of GPP when PAR_{dir} is low. Despite some fluctuations, the underestimation of GPP_MOD and GPP_TL becomes more obvious with the increase in AOD at most sites except XSBN and NMG. The underestimation of GPP_TL is smaller than that of GPP_MOD for large AOD values, which is obvious in YC, CBS, QYZ, DHS, and HB, indicating that the TL-LUE model has lower sensitivity to aerosols than MOD17 at these sites. The reduction in underestimation of TL-LUE is smaller at the three grassland sites (HB, NMG and DX) than at the other sites because the AOD at the grassland sites is low (ranging from 0.1 to 0.4) and the aerosol impact on PAR_{dir} is small.

The RMSE of the estimated GPP shows various tendencies with the

increasing AOD (Fig. 10). The RMSE of the estimated GPP is relatively higher for high AOD values than for low AOD values at the YC, CBS, QYZ and HB sites, which exhibit persistent and increasing underestimation of GPP with the increase in AOD. However, the DHS and XSBN sites have larger RMSE values at low AOD values than that at high AOD values because of the overestimation at low AOD values. Generally, the RMSE of GPP_TL is smaller than that of GPP_MOD, especially for high AOD values. In XSBN, the RMSE of GPP_TL is much smaller than that of GPP_MOD when AOD is less than 0.8, which may be a result of the decrease in both overestimation and underestimation of GPP_TL.

The simulated LUE values of GPP_MOD and GPP_TL exhibit a similar tendency to the observed LUE with the increase in AOD (Fig. 11). However, the simulated LUE is generally smaller than the observed LUE due to the underestimation of GPP at all sites except XSBN. The LUE of GPP_TL is closer to that of GPP_FLUX than GPP_MOD.

The seasonal variation in the averaged bias between the estimated

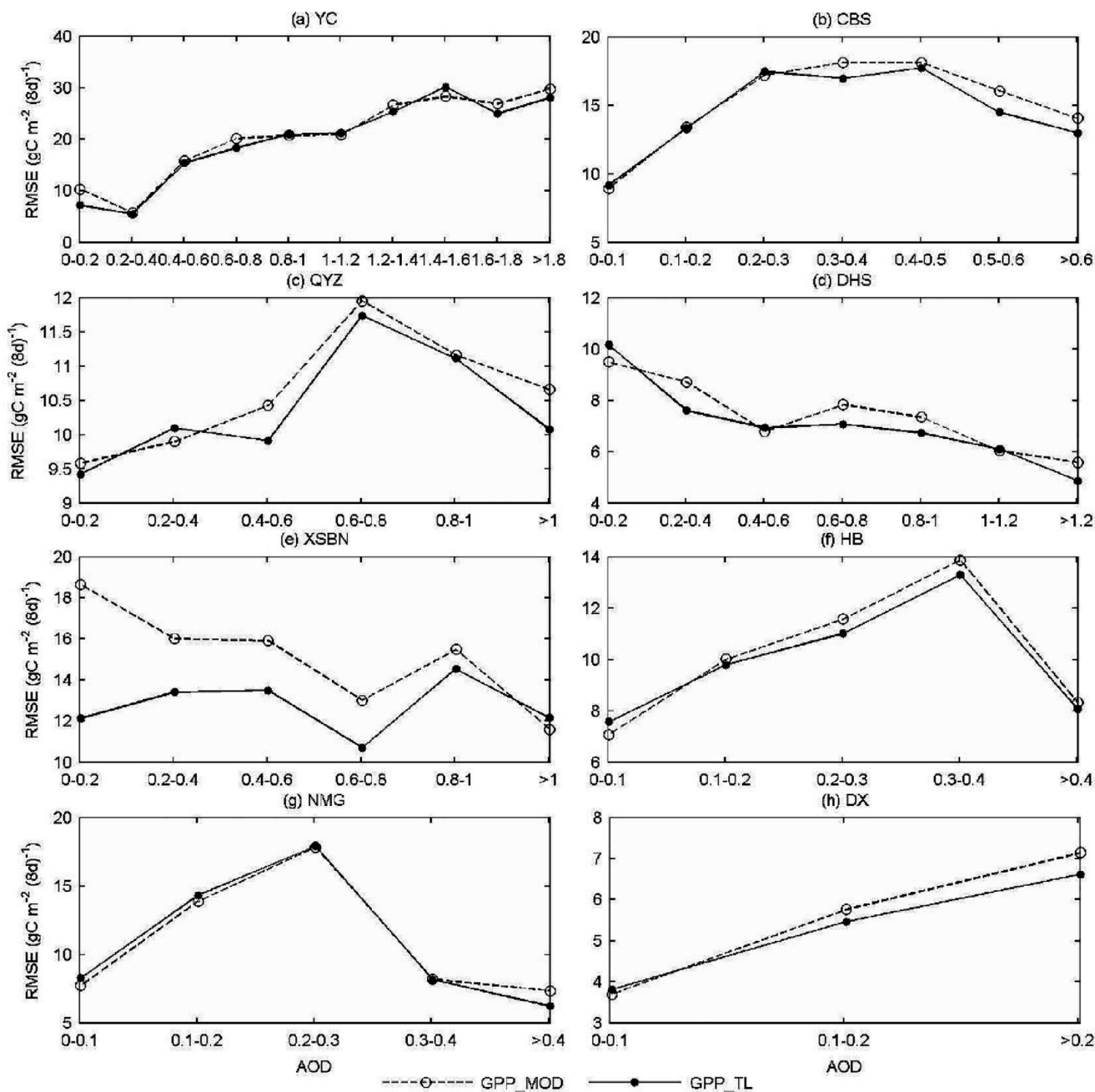


Fig. 10. RMSE between the estimated GPP from two models (MOD17 and TL-LUE) using calibrated parameters and the measured GPP at the ChinaFLUX sites from 2003 to 2010 with the AOD changes.

GPP and the measured GPP Fig. 12 shows that large underestimation of GPP often occurs in the months with high AOD levels at most sites during the corresponding growth period of plants except at XSBN and DHS. Specifically, the underestimation of GPP at YC site is highest in April and August when AOD is high for winter wheat and summer maize, respectively. The growth period of mixed forests at CBS site spans from May to September. The underestimation at CBS reaches a peak in July when AOD is 0.31. The correlation between AOD seasonal variation and underestimation change is insignificant at DHS and XSBN, which are covered by subtropical evergreen broadleaf forest and tropical evergreen broadleaf forest. The reason for this is that the PAR_{dif} variation is also influenced by water vapor change due to dry/wet seasonality in addition to aerosols. The two models show greater underestimation in months with high AOD than in months with low AOD at the evergreen

needleleaf forest site (QYZ). For grassland sites (HB, NMG and DX), the underestimation exhibits obvious consistent tendency with AOD during the growing season of grass (May to September).

5. Conclusions

This study investigated the sensitivity of the MOD17 and TL-LUE models to the PAR_{dif} fraction and AOD. The GPP estimated by the two models (GPP_MOD and GPP_TL) were validated using the measured GPP_FLUX at eight ChinaFLUX sites. Although GPP_MOD and GPP_TL exhibited good agreement with GPP_FLUX, both showed systematic underestimation. Basically, the underestimation of GPP_MOD was larger than that of GPP_TL. The GPP_MOD and GPP_TL showed increasing underestimation with the increasing PAR_{dif} fraction. The TL-LUE model

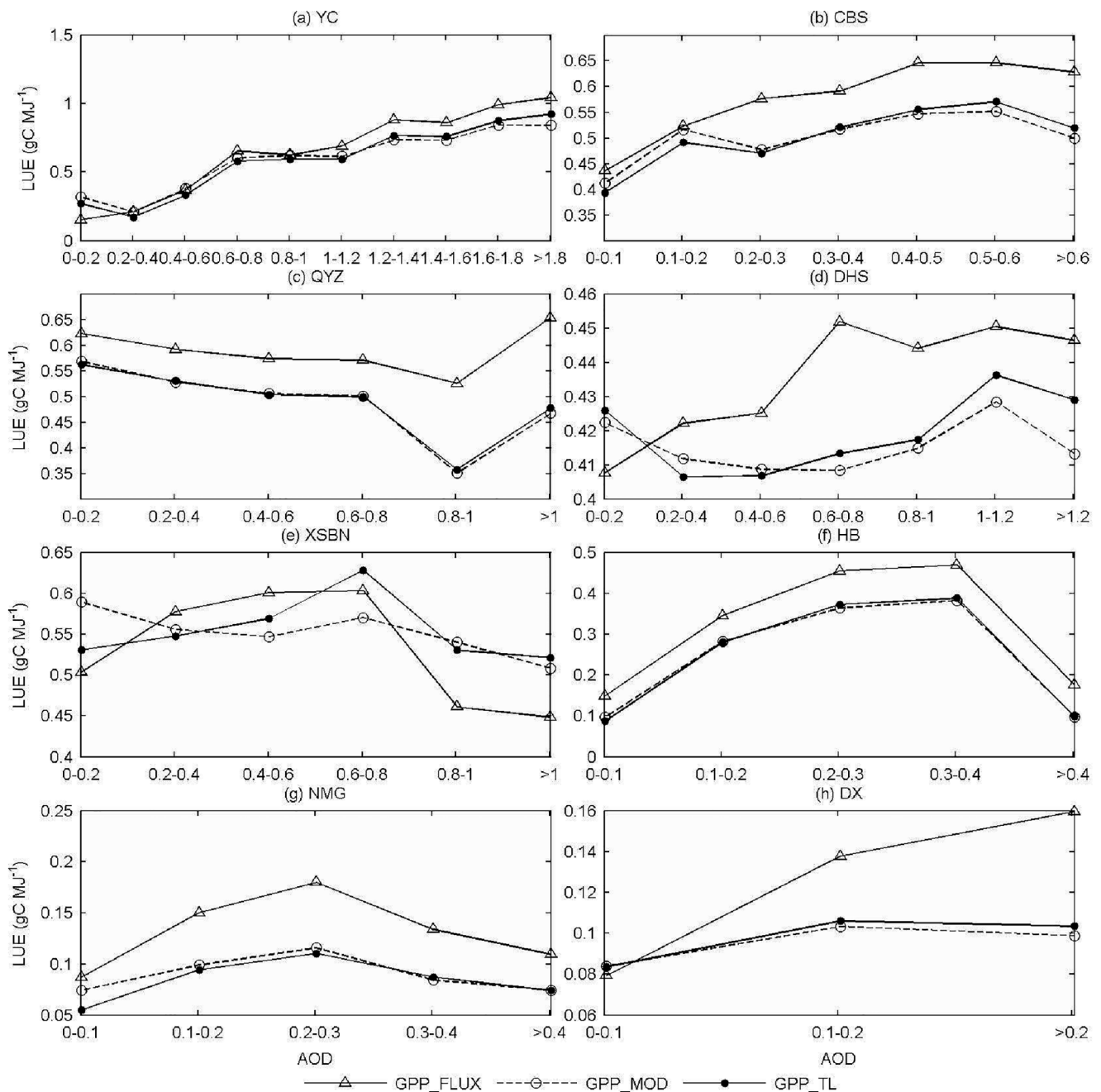


Fig. 11. Dependence of the observed and modelled light use efficiency (LUE) on AOD.

performed better than the MOD17 model with reduced underestimation and decreased RMSE values when the PAR_{dif} fraction was larger than 0.7 or 0.8. However, the TL-LUE model led to a greater underestimation and RMSE at low PAR_{dif} fractions. The seasonal variation in the estimated GPP sensitivity to the PAR_{dif} fraction showed that the underestimation of the estimated GPP from the two models is larger in months with high PAR_{dif} fractions than in those with low PAR_{dif} fractions at most sites. The underestimation of GPP is larger for high AOD values than for low AOD values at most sites. GPP_TL exhibited a smaller underestimation than GPP_MOD. The overestimation also occurred at low AOD values, which is consistent with that for low PAR_{dif} fractions. Therefore, the one-leaf and two-leaf LUE models showed different performances under different PAR_{dif} fractions and AOD conditions, which should be considered for the further improvements of GPP models.

This study provides a guide for improvement of GPP estimation

models. The relationship between LUE and PAR_{dif} should be explored and introduced in LUE models to resolve the underestimations of GPP. The LUE parameters (ϵ_{max} , ϵ_{sun} and ϵ_{sh}) may change with the PAR_{dif} fraction instead of being treated as constants that only depend on species. In addition, the LUE model parameters should be evaluated on a season basis to improve the model performance.

CRedit authorship contribution statement

Xin Li: Conceptualization, Methodology, Writing - original draft, Funding acquisition. **Hongyu Liang:** Supervision, Visualization, Investigation. **Weiming Cheng:** Writing - review & editing.

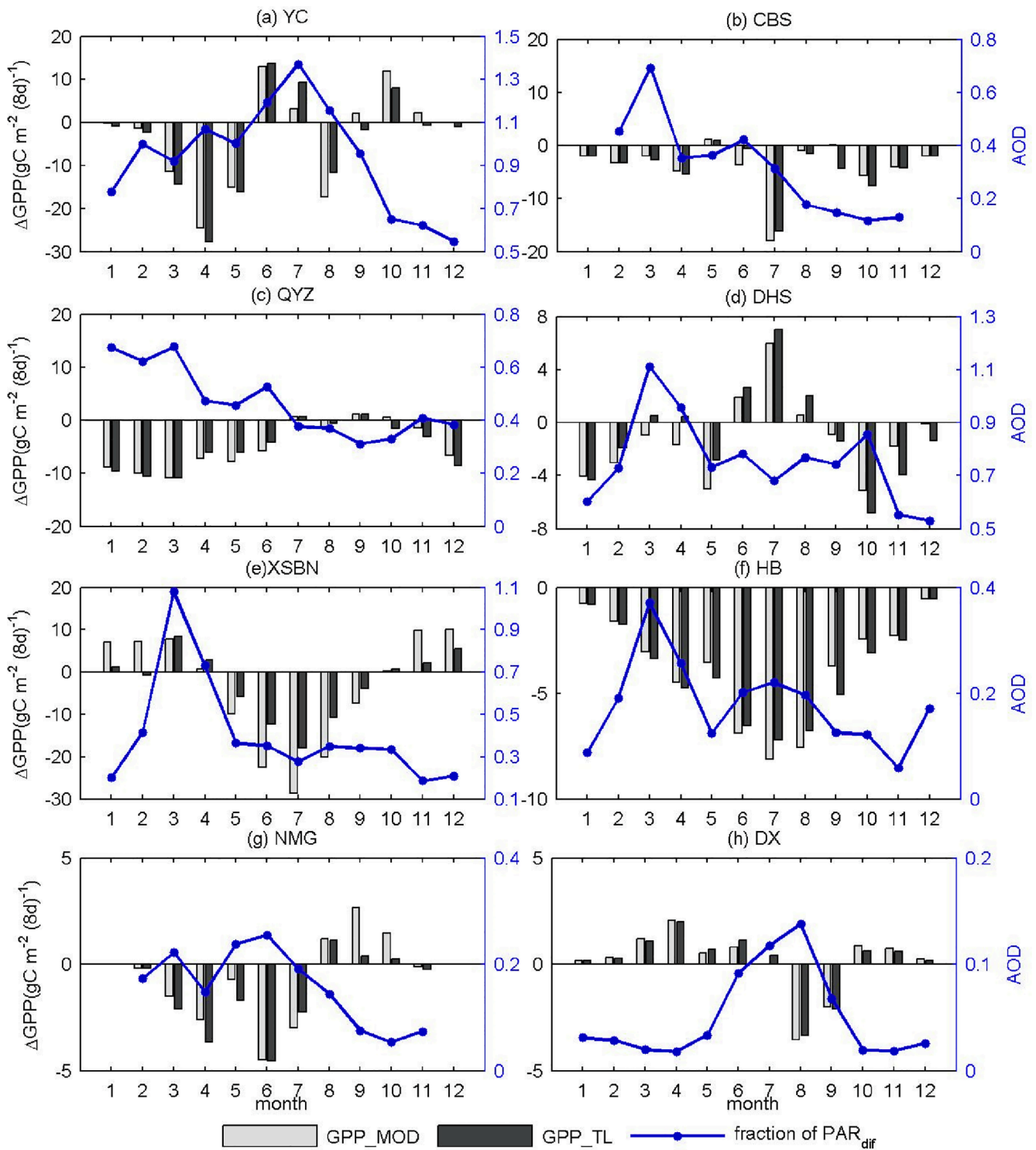


Fig. 12. Seasonal variation in the averaged bias between the estimated GPP (GPP_MOD and GPP_TL) and the measured GPP at ChinaFLUX sites and the averaged AOD during 2003–2010.

Declaration of Competing Interest

The authors declare that they have no known competing financial interests or personal relationships that could have appeared to influence the work reported in this paper.

Acknowledgements

We appreciate ChinaFLUX for providing the tower flux data. This

research was supported by the China Postdoctoral Science Foundation (2019M650830) and Jiangsu Surveying and GIS Science Foundation (JSCHKY201912).

Appendix A. Supplementary material

Supplementary data to this article can be found online at <https://doi.org/10.1016/j.jag.2020.102269>.

References

- Chen, J., Zhang, H., Liu, Z., Che, M., Chen, B., 2014. Evaluating parameter adjustment in the MODIS gross primary production algorithm based on eddy covariance tower measurements. *Remote Sens.* 6, 3321–3348.
- Chen, J.M., Feng, D., Mingzhen, C., 2006. Locally adjusted cubic-spline capping for reconstructing seasonal trajectories of a satellite-derived surface parameter. *IEEE Trans. Geosci. Remote Sens.* 44, 2230–2238.
- Chen, J.M., Liu, J., Cihlar, J., Goulden, M.L., 1999. Daily canopy photosynthesis model through temporal and spatial scaling for remote sensing applications. *Ecol. Model.* 124, 99–119.
- Cheng, Y.-B., Zhang, Q., Lyapustinc, A.I., Wang, Y., Middleton, E.M., 2014. Impacts of light use efficiency and FPAR parameterization on gross primary production modeling. *Agric. For. Meteorol.* 189–190, 187–197.
- Cohan, D.S., Xu, J., Greenwald, R., Bergin, M.H., Chameides, W.L., 2002. Impact of atmospheric aerosol light scattering and absorption on terrestrial net primary productivity. *Global Biogeochem. Cycles* 16, 37–31–37–12.
- Dong, T., Wu, B., Meng, J., Du, X., Shang, J., 2016. Sensitivity analysis of retrieving fraction of absorbed photosynthetically active radiation (FPAR) using remote sensing data. *Acta Ecologica Sinica* 36, 1–7.
- He, M., Ju, W., Zhou, Y., Chen, J., He, H., Wang, S., et al., 2013. Development of a two-leaf light use efficiency model for improving the calculation of terrestrial gross primary productivity. *Agric. For. Meteorol.* 173, 28–39.
- Kumar, S., Kumar, S., 2017. Impact of aerosol on climate and productivity of rice and wheat crop in Bihar. *J. Agrometeorology* 19, 23–28.
- Li, X., Liang, H., Cheng, W., 2020. Spatio-temporal variation in AOD and correlation analysis with PAR and NPP in China from 2001 to 2017. *Remote Sensing* 12, 976.
- Liu, Z., Shao, Q., Liu, J., 2014. The performances of MODIS-GPP and -ET products in china and their sensitivity to input data (FPAR/LAI). *Remote Sens.* 7, 135–152.
- Lloyd, J., Taylor, J.A., 1994. On the temperature dependence of soil respiration. *Funct. Ecol.* 8, 315–323.
- Monteith, J.L., 1972. Solar radiation and productivity in tropical ecosystems. *J. Appl. Ecol.* 9, 747–766.
- Rap, A., Scott, C.E., Reddington, C.L., Mercado, L., Ellis, R.J., Garraway, S., et al., 2018. Enhanced global primary production by biogenic aerosol via diffuse radiation fertilization. *Nat. Geosci.* 11, 640–644.
- Running, S., Mu, Q., Zhao, M., 2015. MOD17A2H MODIS/Terra Gross Primary Productivity 8-Day L4 Global 500m SIN Grid V006. In: NASA EOSDIS Land Processes DAAC.
- Running, S.W., Thornton, P.E., Nemani, R., Glassy, J.M., 2000. Global terrestrial gross and net primary productivity from the earth observing system. *Methods in ecosystem scienc.* Springer, New York, NY.
- Sabtraftar, K., Mackey, B., Croke, B., 2011. Sensitivity of modelled gross primary productivity to topographic effects on surface radiation: a case study in the Cotter River Catchment, Australia. *Ecol. Model.* 222, 795–803.
- Stocker, B.D., Zscheischler, J., Keenan, T.F., Prentice, I.C., Seneviratne, S.I., Peñuelas, J., 2019. Drought impacts on terrestrial primary production underestimated by satellite monitoring. *Nat. Geosci.* 12, 264–270.
- Strada, S., Unger, N., Yue, X., 2015. Observed aerosol-induced radiative effect on plant productivity in the eastern United States. *Atmos. Environ.* 122, 463–476.
- Sun, Z., Wang, X., Zhang, X., Tani, H., Guo, E., Yin, S., et al., 2019. Evaluating and comparing remote sensing terrestrial GPP models for their response to climate variability and CO2 trends. *Sci. Total Environ.* 668, 696–713.
- Tramontana, G., Ichii, K., Camps-Valls, G., Tomelleri, E., Papale, D., 2015. Uncertainty analysis of gross primary production upscaling using Random Forests, remote sensing and eddy covariance data. *Remote Sens. Environ.* 168, 360–373.
- Turner, D.P., Ritts, W.D., Cohen, W.B., Gower, S.T., Running, S.W., Zhao, M., et al., 2006. Evaluation of MODIS NPP and GPP products across multiple biomes. *Remote Sens. Environ.* 102, 282–292.
- Wagle, P., Xiao, X., Torn, M.S., Cook, D.R., Matamala, R., Fischer, M.L., et al., 2014. Sensitivity of vegetation indices and gross primary production of tallgrass prairie to severe drought. *Remote Sens. Environ.* 152, 1–14.
- Wang, S., Huang, K., Yan, H., Yan, H., Zhou, L., Wang, H., et al., 2015. Improving the light use efficiency model for simulating terrestrial vegetation gross primary production by the inclusion of diffuse radiation across ecosystems in China. *Ecol. Complexity* 23, 1–13.
- Xie, X., Li, A., Jin, H., Tan, J., Wang, C., Lei, G., et al., 2019. Assessment of five satellite-derived LAI datasets for GPP estimations through ecosystem models. *Sci. Total Environ.* 690, 1120–1130.
- Yan, H., Wang, S.-Q., Yu, K.-L., Wang, B., Yu, Q., Bohrer, G., et al., 2017. A novel diffuse fraction-based two-leaf light use efficiency model: an application quantifying photosynthetic seasonality across 20 AmeriFlux flux tower sites. *J. Adv. Model. Earth Syst.* 9.
- Yuan, W., Cai, W., Xia, J., Chen, J., Liu, S., Dong, W., et al., 2014. Global comparison of light use efficiency models for simulating terrestrial vegetation gross primary production based on the LaThuile database. *Agric. For. Meteorol.* 192–193, 108–120.
- Zan, M., Zhou, Y., Ju, W., Zhang, Y., Zhang, L., Liu, Y., 2018. Performance of a two-leaf light use efficiency model for mapping gross primary productivity against remotely sensed sun-induced chlorophyll fluorescence data. *Sci. Total Environ.* 613–614, 977–989.
- Zhou, Y., Wu, X., Ju, W., Chen, J.M., Wang, S., Wang, H., et al., 2016. Global parameterization and validation of a two-leaf light use efficiency model for predicting gross primary production across FLUXNET sites. *J. Geophys. Res. Biogeosci.* 121, 1045–1072.
- Zhu, X., He, H., Ma, M., Ren, X., Zhang, L., Zhang, F., et al., 2020. Estimating ecosystem respiration in the grasslands of northern china using machine learning: model evaluation and comparison. *Sustainability* 12, 2099.